Ultrafast single-shot optical vector network analyzer based on coherent time-stretch

Cite as: APL Photon. 5, 106109 (2020); doi: 10.1063/5.0022121
Submitted: 17 July 2020 • Accepted: 6 October 2020 •
Published Online: 15 October 2020

A. Lun Li,[1] B. Liang Xu,[1] C. Sidong Fu,[1] D. Lei Zhang,[1] E. Yuhua Duan,[1] F. Yaoshuai Li,[1] G. Ningning Yang,[1] H. Yu Yu,[1] I. Chi Zhang,[1,a)] J. Kenneth K. Y. Wong,[2] and K. Xinliang Zhang[1]

AFFILIATIONS

[1]Wuhan National Laboratory for Optoelectronics, Huazhong University of Science and Technology, Wuhan 430074, China
[2]Department of Electrical and Electronic Engineering, The University of Hong Kong, Pokfulam Road, Hong Kong

[a)]**Author to whom correspondence should be addressed:** chizheung@hust.edu.cn

ABSTRACT

Ever-increasing demands for a higher bandwidth of data in the optical communications augment the operating frequency of components and systems. To accelerate the development of these large-bandwidth technologies, there is a growing demand to characterize the frequency response of optical devices in real time. In this work, we report a method to significantly improve the measurement speed of an optical vector network analyzer (OVNA) with coherent time-stretch (CTS). Single-shot frequency spectrum measurements are enabled by time-stretch technology that maps the spectrum of an optical pulse to the time domain. Compared to single-ended detection, the implementation of coherent detection enables the acquiring of accurate phase information of the signal and also provides the digital processed cancellation of dispersion-induced impairments. By utilizing dispersive time-stretch and digital coherent detection techniques, we demonstrate an ultrafast and wide bandwidth OVNA. We successfully characterize its performance by measuring the frequency response of a micro-ring cavity and a silicon Mach–Zehnder interferometer with 0.07-nm spectral resolution and 0.156-rad phase accuracy over 10-nm bandwidth. Meanwhile, the dynamic responses of the magnitude and phase, and the drift of the resonance wavelength of the micro-ring modulator under thermal tuning, were fully recorded by the CTS-OVNA at a 20-MHz frame rate.

I. INTRODUCTION

Real-time measurement of the magnitude and phase responses of an optical component plays a critical role in both components' characterization and optical system design, and similar to the electrical domain, it is usually known as the optical vector network analyzer (OVNA). Conventionally, several approaches are introduced to realize the OVNA, such as the modulation phase-shift approach,[1,2] the interferometry approach,[3] and the optical single-sideband (OSSB) modulation approach.[4–6] Meanwhile, to characterize the optical multi-port devices, the spatially diverse optical vector network analyzer is also proposed.[7] However, the interferometry-based OVNA and phase-shift-based OVNA inherently have a relatively low spectral resolution and long measurement time owing to the low wavelength accuracy and poor stability of the wavelength-swept laser sources required in the schemes.[8–11] In addition, the modulation phase-shift approach only measures the group delay rather than the phase of the optical transfer function.[12] To enhance the performance of scanning accuracy, the OVNA based on OSSB modulation was proposed and demonstrated.[4–6,8–10] Benefiting from the high-resolution frequency sweeping and accurate magnitude and phase detection in the electrical domain, the resolution of the OSSB-based OVNA can reach hundreds of kilohertz, with the frame rate in several hertz range.[11] However, the measurement bandwidth of the OVNA is usually limited by the bandwidth of the optoelectronic devices and resolution constraints. To extend the measurement bandwidth of the OVNA, an optical frequency comb was introduced to replace the swept-laser, and 8-nm bandwidth and 334-Hz resolution were demonstrated, while its acquisition frame rate was still in several hertz range.[13] Therefore, the aforementioned approaches are not able to measure the ultrafast dynamics of some optical components.[11–14] Meanwhile, the longer frequency response measurement time also results in higher costs, and a faster testing approach is expected.[15]

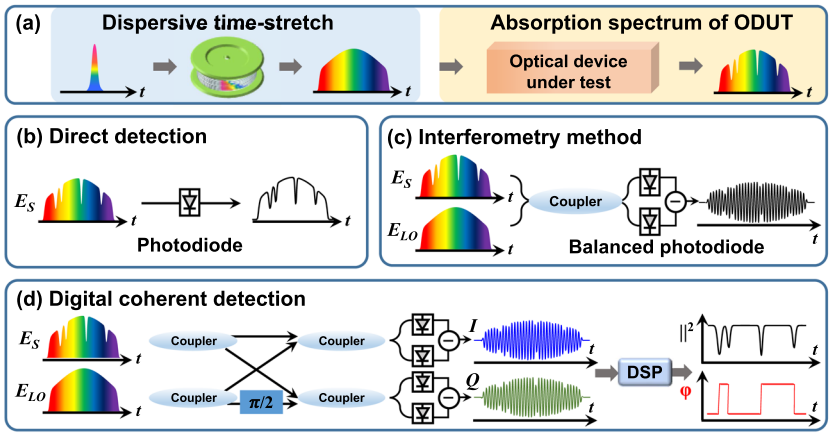

FIG. 1. (a) Absorption spectrum captured by time-stretch spectroscopy. (b) Direct detection and (c) interferometry method for the time-stretch spectroscopy. (d) Digital coherent detection is applied to retrieve the full-field information. LO, local oscillator; DSP, digital signal processing.

To improve the acquisition time resolution, ultrafast spectroscopy based on dispersive time-stretch has attracted a lot of attention, as shown in Fig. 1(a). After mapping the spectrum of an optical pulse to the time domain, the spectrum can be captured by a single-pixel detector and a real-time oscilloscope with tens of MHz frame rate.[16–19] By virtue of its ultrafast frame rate, dispersive time-stretch technology has been employed for the discovery of many ultrafast measurements, such as optical rogue waves[20] and the buildup of mode-locking.[21–23] Meanwhile, a dispersive time-stretch technique is applied to enable an extremely fast measurement of the frequency response of electronic devices.[14,15,24] Although the spectral intensity profile can be acquired in real time by direct detection [Fig. 1(b)], the spectral phase information cannot be retrieved without complex intervention and algorithms.[14,15] To acquire the optical phase information in a more straightforward way, the interferometry method was introduced to the conventional dispersive time-stretch, as shown in Fig. 1(c).[25] Here, a Hilbert transform was performed to extract the phase information from the data of a single-pixel photodetector to achieve microscopic imaging. However, there is an assumption that the intensity of the signal and reference is varying with time slowly; thus, the Hilbert transform can provide an approximation to a proper phase.[26] To improve the detection sensitivity and eliminate the noise generated in system, a balanced photodiode (BPD) is introduced to achieve the extraction of the intermediate frequency (IF).[27] Without phase-diversity being applied in balanced detection, a Hilbert transform is still required to extract the phase and IF. To improve the extracting phase accuracy of the time-stretch-based OVNA, an optical digital coherent detection technique is introduced here, as shown in Fig. 1(d). A similar approach has been applied in an ultrafast microscope system to retrieve the phase and polarization information of the images.[28,29] The phase and polarization diversity of the homodyne receiver eliminates the influence of signal intensity and polarization fluctuation, and the accurate magnitude and phase responses can be reconstructed by digitizing the in-phase (I) and quadrature-phase (Q) signals from a phase-diversity homodyne receiver, and then, it reconstructs the full-field optical waveform using digital signal processing (DSP).[30–36]

With the combination of the dispersive time-stretch and digital coherent detection techniques, we propose a coherent time-stretch based optical vector network analyzer (CTS-OVNA) to enable the single-shot measurement of the magnitude and phase responses of an optical component by mapping different optical frequency components to different temporal positions. The chirped optical pulse propagates through the optical device under test (ODUT) in which the magnitude and phase of the signal are changed according to the spectral responses of the ODUT. The measurement frame rate is equivalent to the repetition rate of the pulse laser (~20 MHz), and under this 50-ns acquisition period, this ultrafast CTS-OVNA achieves a spectral resolution of 0.07 nm, a phase accuracy of 0.156 rad, and a observation bandwidth of over 10 nm. Meanwhile, the frequency responses of a silicon Mach–Zehnder interferometer (MZI) and a micro-ring cavity have been successfully characterized by the CTS-OVNA, and the measurement results correspond consistently with the optical spectrum analyzer (OSA). Moreover, the spectro-temporal dynamics of the thermal tuning micro-ring modulator was directly observed over long record lengths of ~1000 consecutive pulses, around 50 μs.

II. PRINCIPLE AND THEORETICAL ANALYSIS

Figure 1 illustrates the schematic of the CTS-OVNA. The optical pulse train goes through the dispersive element to achieve wavelength-to-time mapping, and by passing through the ODUT, its absorption spectrum is thus encoded on the time axis. As shown in Fig. 1(b), the most conventional direct detection only extracts the signal intensity envelope, and the bottleneck lies in the square law detectors that filter out all fast phase variation. Then, the interferometry method is introduced to recover the phase information, as illustrated in Fig. 1(c). An identical chirped reference beam mixes with the absorption spectrum under test, and Hilbert transformation is then performed on the interference signal such that the approximate phase information can be obtained. As Fig. 1(d) illustrates, with the phase-diversity being employed, the chirped local oscillator (LO) passes through a 90° hybrid and interferes with the signal to generate in-phase and quadrature-phase signals in the coherent receiver. After the optical-to-electrical signal conversion, the digitizer is used to sample and quantify the analog signal. Then, the signals (I and Q) are sent to the DSP unit and processed to obtain the

magnitude and phase responses of the ODUT. An analysis of the principles of dispersive time-stretch and digital coherent detection is provided as follows.

A. Dispersive time-stretch

Dispersive time-stretch is also known as dispersive Fourier transformation (DFT),[37–39] which is a powerful method that overcomes the speed limitation of conventional spectroscopy and permits the single-shot measurements of rapidly evolving spectral dynamics. In this CTS-OVNA system, the dispersive time-stretch is performed by the dispersion compensating fiber (DCF) with the total group velocity dispersion (GVD) of D_{total} = 4 ns/nm, and the spectral resolution can be expressed as

$$\delta_\lambda = \lambda \cdot \sqrt{\frac{2}{D_{total} \cdot c}}, \quad (1)$$

where c is the speed of light and λ is the center wavelength, and it achieved 0.07-nm spectral resolution.[37] It is desirable to increase the amount of dispersion to improve resolution and reduce the acquisition bandwidth requirement, but to avoid the overlapping between neighboring pulses, the maximum temporal dispersion of DCF is limited by the period of the pulse laser (T) and the spectral bandwidth ($\Delta\lambda$), and it can be described as $D_{total} \cdot \Delta\lambda < 1/T$. Therefore, it is necessary to select the appropriate amount of GVD to avoid pulse overlap and provide good spectral resolution.

B. Digital coherent receiver

The digital coherent detection measures the magnitude and phase responses by digitizing the I and Q signals from a phase-diversity homodyne receiver[34,35] and then reconstructing the optical waveform using DSP.[33] Figure 1(d) illustrates a typical phase-diversity coherent receiver. The LO is divided into two arms to beat with the two paths of the signal, respectively. One of the LO arms is phase shifted by 90° so that the quadrature components can be detected simultaneously. The currents from two BPDs are given as

$$I_I(t) = k\times 4A_S(t)A_{LO}(t)\cos[(\omega_S - \omega_{LO})t + \varphi_S(t) - \varphi_{LO}(t)], \quad (2)$$

$$I_Q(t) = k\times 4A_S(t)A_{LO}(t)\sin[(\omega_S - \omega_{LO})t + \varphi_S(t) - \varphi_{LO}(t)], \quad (3)$$

where k is the responsivity of the photodetectors, $A_S(t)$ is the amplitude of the signal, $A_{LO}(t)$ is the amplitude of the LO light, $\varphi_S(t)$ and $\varphi_{LO}(t)$ are the phase of the signal and LO, respectively, and ω_S and ω_{LO} are the optical carrier frequencies of the signal and LO, respectively. Then, the complex amplitude in digital signal processing can be expressed as

$$\begin{aligned} I_C(t) &= I_I + jI_Q \\ &= k\times 4A_S(t)A_{LO}(t) \\ &\quad \times \exp\{j(\omega_S - \omega_{LO})t + j[\varphi_S(t) - \varphi_{LO}(t)]\}. \end{aligned} \quad (4)$$

Through DSP, the magnitude response can be obtained, and the phase information containing the frequency difference between the signal and LO can be solved as $\tan^{-1}|I_Q|/|I_I|$.[29]

III. EXPERIMENTAL SETUP

The detailed experimental setup of the real-time ultrafast OVNA is shown in Fig. 2. A mode-lock laser generates a 20-MHz optical pulse train, which is chirped by passing through a dispersive fiber with ~4-ns/nm GVD (compensating 240-km SMF). An erbium-doped fiber amplifier (EDFA) boosts up the chirped pulse train to 20-dBm (average power), before an optical bandpass filter with 12-nm bandwidth. After that, a 1 × 2 optical coupler separates the pulses into the signal arm and the reference arm. In the signal arm, the stretched pulses pass through the ODUT, as well as another EDFA to compensate its insertion loss. An optical variable delay line is applied in the reference arm to fine tune the relative time delay between two arms, and ~4-GHz frequency offset is achieved,[25,27,28] which should be below the bandwidth of the coherent receiver (Finisar, CPRV1225). In the coherent receiver, the optical signal is combined with the reference beam. The LO generated in the reference arm is designed to have higher power than the signal to enhance the sensitivity. A real-time oscilloscope (operated at

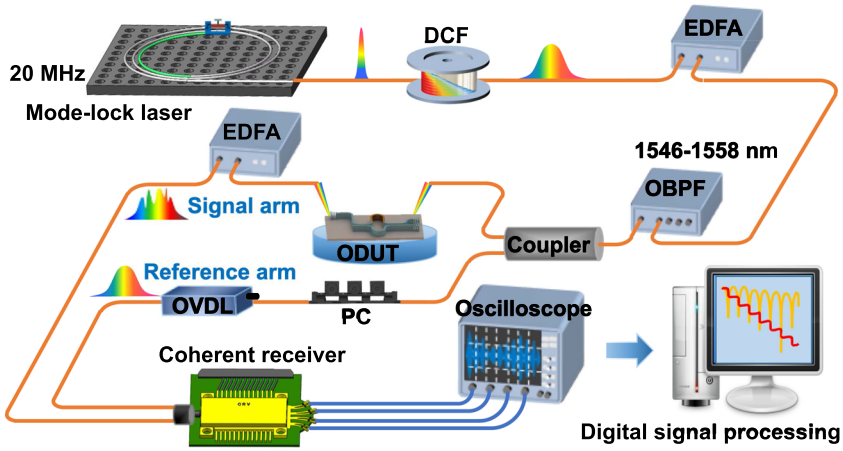

FIG. 2. Experimental setup of the CTS-OVNA. DCF, dispersion compensation fiber; EDFA, erbium-doped fiber amplifier; OBPF, optical bandpass filter; PC, polarization controller; ODUT, optical device under test; OVDL, optical variable delay line.

80 GS/s) acquires the I and Q data from the receiver, which can be used to recover the phase and magnitude information of the ODUT by DSP.

IV. DIGITAL SIGNAL PROCESSING

As shown in Fig. 3, the flow chart of DSP mainly consists of five steps: (1) subtract the complementary outputs; (2) recover the full field signal; (3) remove the IF; (4) extract the magnitude and phase response; and (5) calibrate the responses of the ODUT. The system noise is first eliminated by subtracting the complementary outputs from a phase-diversity homodyne receiver, and the full field signal is recovered from the I and Q signals. Next, the full field signal is processed to remove IF and eliminate the out-of-band noise by a low-pass filter. The magnitude response of the ODUT is achieved via dividing the magnitude envelope of the ODUT by the magnitude envelope of LO signal. The $\tan^{-1}|I_Q|/|I_I|$ is then performed to extract the phase information of the ODUT. To further increase the accuracy of the measurement, the instrument response of system should be taken into account, including the gain flatness and the link dispersion. The calibration parameters of magnitude and phase can be obtained by removing the ODUT. Finally, an accurate frequency response of the ODUT can be achieved by utilizing the calibration parameters to eliminate disturbances introduced by the instruments of the system.

V. EXPERIMENTAL RESULTS AND DISCUSSIONS

To demonstrate the capability of the CTS-OVNA for obtaining magnitude and phase responses, a waveshaper (Finisar, 1000s) was placed as the ODUT, which was configured to have deliberate intensities and phase profiles as the red dashed lines shown in Figs. 4(a) and 4(b). To clearly compare with the experimental results, the results of measuring by an OSA and simulation are shifted by 18 dB and 3.5 rad, respectively. As illustrated in Figs. 4(a) and 4(b), the measured magnitude and phase (black solid lines) are consistent with the result measured by the OSA and simulation (red dashed lines). It is noted that the calibration parameters of magnitude and phase are obtained by setting up the waveshaper as an all-pass filter with transparent phase, and it can effectively calibrate the system profile during the subsequent DSP.

The magnitude information of the waveshaper was designed to have different spectral intervals, which were 0.1 nm, 0.2 nm, and 0.3 nm, respectively. As illustrated in Fig. 4(a), the actual spectral resolution of the waveshaper is worse than 0.1 nm, therefore, the 0.1-nm spectral interval signal cannot be effectively generated. As shown in Fig. 4(b), to explore the phase sensitivity of the system, the phase profile with different peak values (~0.156 rad) is applied, and this small phase difference can be also retrieved accurately by CTS-OVAN.

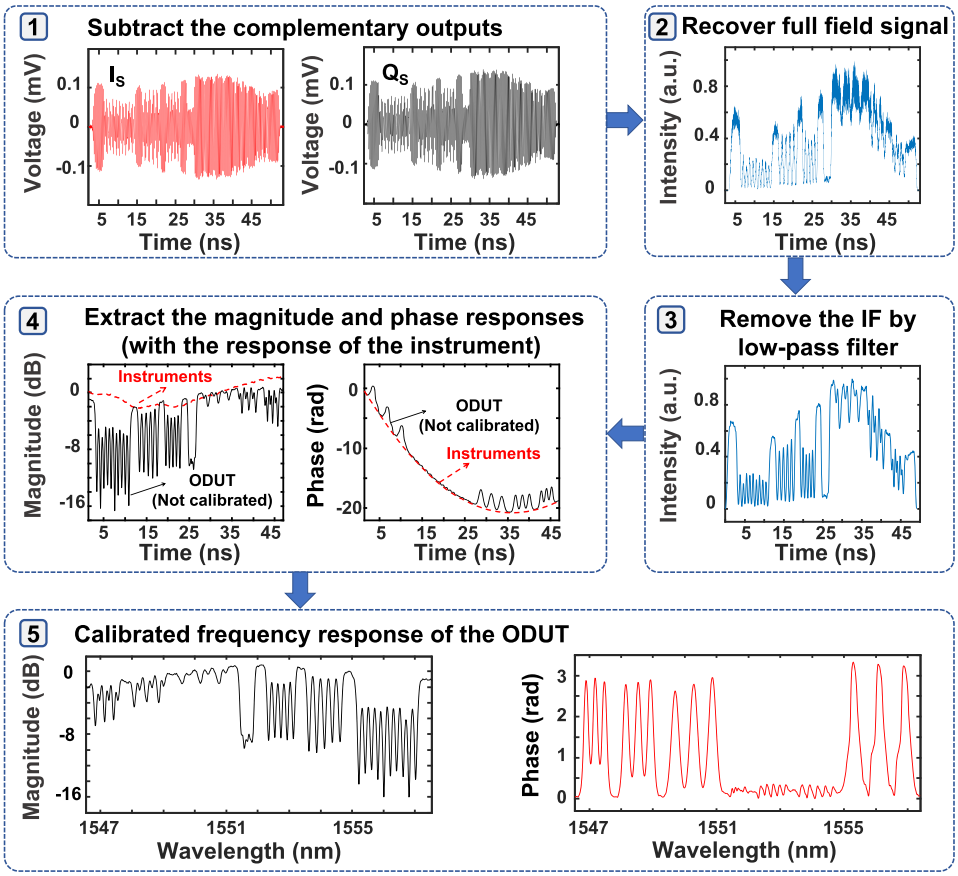

FIG. 3. Flow chart of the digital signal processing.

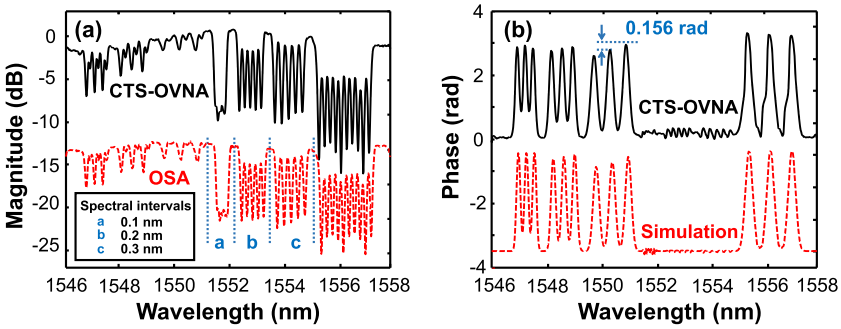

FIG. 4. Performance of the CTS-OVNA with the given magnitude and phase pattern. (a) The magnitude response of the signal programmed on the waveshaper is measured by the CTS-OVNA (black solid line) and an OSA (red dashed line). (b) The phase response obtained by the CTS-OVNA (black solid line), and the phase pattern simulated from the driving signal of the waveshaper (red dashed line).

To further characterize the real-time performance of the system, the CTS-OVNA was applied to measure the frequency response of silicon devices. First, the CTS-OVNA was applied to measure the frequency response of a silicon MZI, and the magnitude and phase information over a 10-nm observation bandwidth was provided in Figs. 5(a) and 5(b), respectively. To clearly compare with the experimental results, the results of measuring by an OSA and simulation are shifted by 20 dB and 40 rad, respectively. These figures illustrate the measured phase response with a difference of π and the periodic phase jumps and the free spectral range (FSR) of nearly 200 GHz. As a reference, the magnitude response of the ODUT measured by an OSA is shown by the red dashed line in Fig. 5(a). The phase frequency response of the ODUT is given by the simulation, which is shown by the red-dashed line in Fig. 5(b). Comparing the CTS-OVNA measured results with the reference, the CTS-OVNA measurement matched well with the OSA and simulation results. It could be observed that the signal to noise ratio (SNR) of the measured frequency responses in the marginal areas is lower than that in the middle because the signal in those areas has less power. Similarly, the accuracy of the phase response information is also worse in the marginal areas. However, it is worth mentioning that the measured magnitude and phase information appear slightly different from the OSA measurement results and simulation because the fiber length of the measurement system is longer, and the environmental temperature and mechanical jitter will disturb the system measurement.

To experimentally verify the simulation results of a micro-ring cavity, the magnitude and phase responses of a micro-ring cavity was measured by the CTS-OVNA with an 8-nm observation bandwidth, which are shown in Figs. 6(a) and 6(b). To clearly compare with the experimental results, the results of measuring by an OSA and simulation are shifted by 10 dB and ~2.5 rad, respectively. Compared to the spectrum acquired from OSA and simulation [red dashed line in Figs. 6(a) and 6(b)], the CTS-OVNA measurement matched well

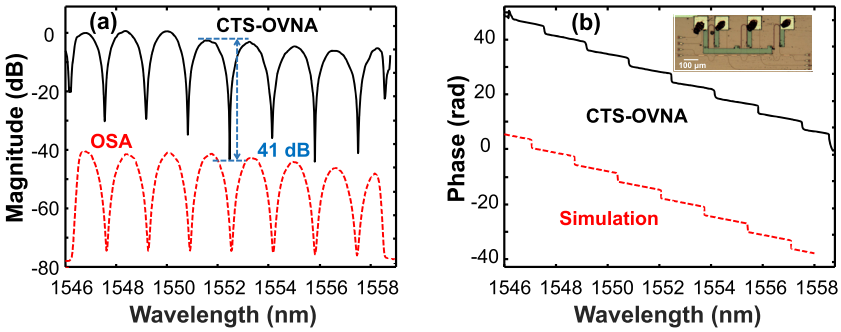

FIG. 5. Full-field response of a silicon Mach–Zehnder interferometer. (a) The magnitude response is measured by the CTS-OVNA (black solid line) and an OSA (red dashed line). (b) The phase response obtained by the CTS-OVNA (black solid line) and simulation result (red dashed line). The inset shows the micrograph of the silicon MZI.

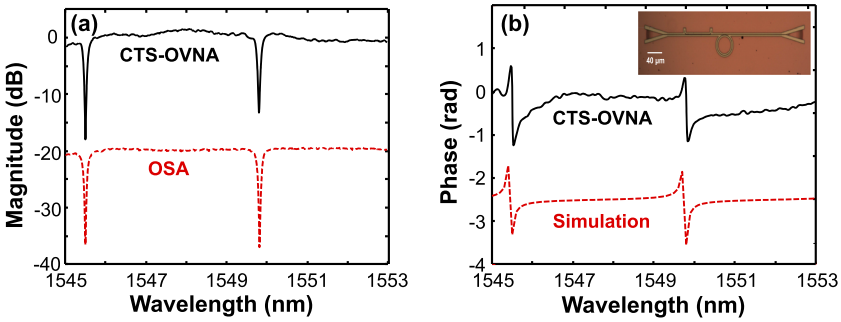

FIG. 6. Full-field response of a micro-ring cavity by the CTS-OVNA. (a) The magnitude response is measured by the CTS-OVNA (black solid line) and an OSA (red dashed line). (b) The phase response obtained by the CTS-OVNA (black solid line) and simulation result (red dashed line). The inset shows the micrograph of the micro-ring cavity.

with the OSA and simulation results. We can see the top of magnitude response has a slight fluctuation. This is because the micro-ring cavity has a wider FSR than MZI and is easily affected by noise.[12] The phase shifts less than π indicates a state of undercoupling.[40] No matter MZI or micro-ring cavity, our experiment results are in agreement with the simulation ones, which confirm the feasibility of our method.

Owing to the relatively high thermo-optic coefficient of silicon,[41] thermal tuning is often applied using a metallic micro-heater on a silicon waveguide in tunable silicon micro-ring resonators.[42,43] During the thermal tuning process, it will cause frequency shift to achieve different applications, such as the differentiator, and the response time can reach microseconds, even the nanosecond level.[44] Therefore, it is meaningful to observe the dynamic response of silicon devices.

To demonstrate the ultrafast real-time measurement capability of the CTS-OVNA, we used the system to capture the thermo-optical dynamics of the micro-ring modulator, which is on a silicon-on-isolator wafer, with a 220-nm-thick top silicon layer and a 2 μm SiO_2 buried oxide (BOX) layer. An external scanning voltage was applied to the heater of the micro-ring modulator to change the power, thereby achieving thermal tuning, and the dynamic responses of the magnitude and phase were measured by the varying power of the heater. The frequency of the radio frequency (RF) driving signal was set to 50 kHz, and the peak-to-peak voltage (V_{PP}) was 6 V, as shown in Fig. 7(c). The spectro-temporal dynamics of the thermal tuning micro-ring modulator was directly observed on a single-shot basis, over long record lengths of ~1000 consecutive pulses (around 50 μs), which are only limited by the memory size of the oscilloscope. Owing to the microsecond response time of the micro-ring modulator, one out of every ten snapshots is selected. A single period (~20 μs) was applied to show the shift of the resonance wavelength as the power varies, as well as the dynamic responses of magnitude and phase information of the ODUT. The notch filter with the center wavelength at 1549.50 nm was selected to achieve a fixed reference wavelength. Thus, the drift of the resonance wavelength can be obtained from the temporal spectra by measuring the time shift off the reference notch.

The data stream exhibits the corresponding shift of the resonance wavelength caused by the radio frequency signal changing periodically. As illustrated in Figs. 7(a) and 7(b), we can find that with the increase in the drive signal power, the resonance wavelength of the silicon micro-ring modulator redshifts. Meanwhile, as the drive signal power decreases, the resonance wavelength of the silicon micro-ring modulator blueshifts.

The main reason is that the temperature of the heater will arise along with the increase in the RF power, which will change the effective index of the silicon micro-ring modulator.[45] The magnitude and phase responses of the single frame along the dashed line in Figs. 7(a) and 7(b) are illustrated in Figs. 7(d) and 7(e), respectively. We successfully characterized the dynamic responses of the magnitude and phase information of the ODUT under thermal tuning and also fully recorded the drift of the resonance wavelength under heater power change. This demonstration firmly establishes the ability of the CTS-OVNA to monitor fast dynamical processes in real time.

From the above analysis and experimental characterization, the CTS-OVNA can well characterize the frequency response of these silicon devices, no matter the state of device is static or dynamic. The key advantage of this approach is ~50-ns ultrafast time resolution and ~1.25-THz ultra-wide bandwidth (10 nm in the 1550-nm wavelength band). Small discrepancies between the traces of the measurement by an OSA and the CTS-OVNA may arise from the temperature-induced timing jitter. Since it always requires a large amount of dispersion, the temperature fluctuation of the long optical fiber link would result in variation in the optical path length and laser cavity length; thus, the frequency-to-time mapping relation will be affected under this circumstance.[46]

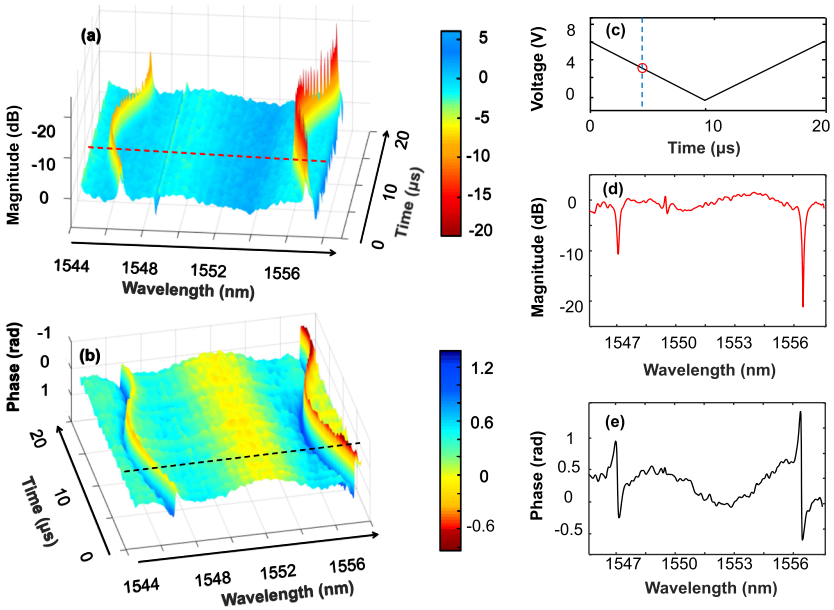

FIG. 7. The thermo-optical dynamics of the micro-ring modulator is captured by the CTS-OVNA. (a) The dynamic magnitude response of the micro-ring modulator with a single period time (~20 μs). (b) The dynamic phase response of the micro-ring modulator obtained by the CTS-OVNA. (c) The waveform of the driving electrical signal with the frequency of 50 kHz, and V_{PP} is 6 V. (d) The magnitude response of the single frame along the red dashed line in (a). (e) The phase response of the single frame along the black dashed line in (b).

With the advance of phase-diversity, the phase information of the ODUT can be accurately extracted, even with the rapid fluctuant intensity profile. Meanwhile, the polarization diversity also enables the digital coherent receiver retrieve the polarization state in real-time. Compared with the conventional OVNA, which requires all the instruments to have large bandwidth, the bandwidth requirements of the CTS-OVNA are greatly relaxed by using the time-stretch technology, and achieves ~50-ns ultrafast acquisition time to monitor fast dynamical processes in real time. Furthermore, compared with the conventional time-stretch spectroscopy, the sensitivity of the CTS-OVNA is also improved due to the high power LO and BPD technique. It is noted that there is still a tradeoff between the measurement range and resolution due to the high acquisition rate. Therefore, it is suggested to localize the region of interest quickly under a wide observation bandwidth and then increase the resolution by introducing large GVD and perform fine observation in smaller bandwidth.

VI. CONCLUSIONS

With the combination of the time-stretch technology and digital coherent detection method, an ultrafast single-shot CTS-OVNA is proposed and experimentally demonstrated. The CTS-OVNA system employed time-stretch technology to achieve frequency-to-time mapping and enhance the speed of measurement. Meanwhile, to improve the accuracy of phase information, a coherent receiver is used to measure the magnitude and phase responses by digitizing the photo-detected I and Q signals from a phase-diversity homodyne receiver. As an initial demonstration, we obtained the magnitude and phase responses by configuring the waveshaper as an ODUT with deliberate intensities and phases profiles, realizing a 0.07-nm spectral resolution and a 0.156-rad phase accuracy. Then, using this system, the frequency responses of a silicon MZI and a micro-ring cavity were obtained over a 10-nm observation bandwidth at a 20-MHz frame rate. Moreover, the dynamic frequency responses and the drift of the resonance wavelength by the micro-ring modulator under thermal tuning were successfully characterized by the CTS-OVNA. The observation range can be improved by decreasing the frame rate. Moreover, its magnitude and phase retrieval algorithm are compatible with the conventional DSP of the coherent detection, and it is promising to be adopted in other application areas.

ACKNOWLEDGMENTS

This work was supported by the National Natural Science Foundation of China (Grant Nos. 61927817, 61735006, and 61675081) and the NSFC/RGC Joint Research Scheme (Grant Nos. 61631166003; N_HKU712/16).

DATA AVAILABILITY

The data that support the findings of this study are available from the corresponding author upon reasonable request.

REFERENCES

[1]T. Niemi, M. Uusimaa, and H. Ludvigsen, "Limitations of phase-shift method in measuring dense group delay ripple of fiber Bragg gratings," IEEE Photonics Technol. Lett. **13**, 1334–1336 (2001).

[2]E. Simova, P. Berini, and C. P. Grover, "Characterization of wavelength-selective fiber-optic devices using a modified phase-shift method," J. Lightwave Technol. **19**, 717–731 (2001).

[3]G. D. Vanwiggeren, A. R. Motamedi, and D. M. Barley, "Single-scan interferometric component analyzer," IEEE Photonics Technol. Lett. **15**, 263–265 (2003).

[4]J. E. Román, M. Y. Frankel, and R. D. Esman, "Spectral characterization of fiber gratings with high resolution," Opt. Lett. **23**, 939–941 (1998).

[5]A. Loayssa, R. Hernández, D. Benito, and S. Galech, "Characterization of stimulated Brillouin scattering spectra by use of optical single-sideband modulation," Opt. Lett. **29**, 638–640 (2004).

[6]M. Sagues and A. Loayssa, "Spectral characterisation of polarisation dependent loss of optical components using optical single sideband modulation," Electron. Lett. **47**, 47–49 (2011).

[7]S. Rommel, J. M. D. Mendinueta, W. Klaus, J. Sakaguchi, J. J. V. Olmos, Y. Awaji, I. T. Monroy, and N. Wada, "Few-mode fiber, splice and SDM component characterization by spatially-diverse optical vector network analysis," Opt. Express **25**, 22347–22361 (2017).

[8]M. Xue, Y. Zhao, X. Gu, and S. Pan, "Performance analysis of optical vector analyzer based on optical single-sideband modulation," J. Opt. Soc. Am. B **30**, 928–933 (2013).

[9]M. Sagues and A. Loayssa, "Swept optical single sideband modulation for spectral measurement applications using stimulated Brillouin scattering," Opt. Express **18**, 17555–17568 (2010).

[10]Z. Tang, S. Pan, and J. Yao, "A high resolution optical vector network analyzer based on a wideband and wavelength-tunable optical single-sideband modulator," Opt. Express **20**, 6555–6560 (2012).

[11]J. Wen, D. Shi, Z. Jia, Z. Shi, M. Li, N. H. Zhu, and W. Li, "Accuracy-enhanced wideband optical vector network analyzer based on double-sideband modulation," J. Lightwave Technol. **37**, 2920–2926 (2019).

[12]Z. Zhang, Y. Dai, L. Yan, K. Xu, Y. Gao, J. Li, Y. Ji, and J. Lin, "A compressed optical vector network analyzer based on two tunable coherent optical frequency combs," in *Asia Communications and Photonics Conference 2013* (Optical Society of America, 2013), p. AF3F.3.

[13]T. Qing, S. Li, Z. Tang, B. Gao, and S. Pan, "Optical vector analysis with attometer resolution, 90-dB dynamic range and THz bandwidth," Nat. Commun. **10**, 5135 (2019).

[14]Z. Bai, C. K. Lonappan, T. Jiang, A. M. Madni, F. Yan, and B. Jalali, "Tera-sample-per-second single-shot device analyzer," Opt. Express **27**, 23321–23335 (2019).

[15]C. K. Lonappan, A. M. Madni, and B. Jalali, "Single-shot network analyzer for extremely fast measurements," Appl. Opt. **55**, 8406–8412 (2016).

[16]J. Chou, D. R. Solli, and B. Jalali, "Real-time spectroscopy with subgigahertz resolution using amplified dispersive Fourier transformation," Appl. Phys. Lett. **92**, 111102 (2008).

[17]D. R. Solli, J. Chou, and B. Jalali, "Amplified wavelength–time transformation for real-time spectroscopy," Nat. Photonics **2**, 48–51 (2008).

[18]C. Zhang, X. Wei, and K. K. Y. Wong, "Performance of parametric spectro-temporal analyzer (PASTA)," Opt. Express **21**, 32111–32122 (2013).

[19]L. Chen, Y. Duan, H. Zhou, X. Zhou, C. Zhang, and X. Zhang, "Real-time broadband radio frequency spectrum analyzer based on parametric spectro-temporal analyzer (PASTA)," Opt. Express **25**, 9416–9425 (2017).

[20]D. R. Solli, C. Ropers, P. Koonath, and B. Jalali, "Optical rogue waves," Nature **450**, 1054–1057 (2007).

[21]A. F. J. Runge, N. G. R. Broderick, and M. Erkintalo, "Observation of soliton explosions in a passively mode-locked fiber laser," Optica **2**, 36–39 (2015).

[22]G. Herink, B. Jalali, C. Ropers, and D. R. Solli, "Resolving the build-up of femtosecond mode-locking with single-shot spectroscopy at 90 MHz frame rate," Nat. Photonics **10**, 321–326 (2016).

[23]G. Herink, F. Kurtz, B. Jalali, D. R. Solli, and C. Ropers, "Real-time spectral interferometry probes the internal dynamics of femtosecond soliton molecules," Science **356**, 50–54 (2017).

[24]Z. Bai, C. K. Lonappan, A. M. Madni, and B. Jalali, "Time-stretch network analyzer for single-shot characterization of electronic devices," in *Conference on Lasers and Electro-Optics* (Optical Society of America, 2019), p. AF3K.6.

[25]A. K. S. Lau, T. T. W. Wong, K. K. Y. Ho, M. T. H. Tang, A. C. S. Chan, X. Wei, E. Y. Lam, H. C. Shum, K. K. Y. Wong, and K. K. Tsia, "Interferometric time-stretch microscopy for ultrafast quantitative cellular and tissue imaging at 1 μm," J. Biomed. Opt. **19**, 076001 (2014).
[26]E. Gengel and A. Pikovsky, "Phase demodulation with iterative Hilbert transform embeddings," Signal Process. **165**, 115–127 (2019).
[27]B. W. Buckley, A. M. Madni, and B. Jalali, "Coherent time-stretch transformation for real-time capture of wideband signals," Opt. Express **21**, 21618–21627 (2013).
[28]L. Song, Y. Feng, X. Guo, Y. Shen, D. Wu, Z. Wu, C. Zhou, L. Zhu, S. Gao, W. Liu *et al.*, "Ultrafast polarization bio-imaging based on coherent detection and time-stretch techniques," Biomed. Opt. Express **9**, 6556–6568 (2018).
[29]Y.-H. Feng, X. Lu, L. Song, X. Guo, Y. Wang, L. Zhu, Q. Sui, J. Li, K. Shi, and Z. Li, "Optical digital coherent detection technology enabled flexible and ultra-fast quantitative phase imaging," Opt. Express **24**, 17159–17167 (2016).
[30]F. N. Hauske, M. Kuschnerov, B. Spinnler, and B. Lankl, "Optical performance monitoring in digital coherent receivers," J. Lightwave Technol. **27**, 3623–3631 (2009).
[31]Y. Painchaud, M. Poulin, M. Morin, and M. Têtu, "Performance of balanced detection in a coherent receiver," Opt. Express **17**, 3659–3672 (2009).
[32]M. S. Faruk, Y. Mori, C. Zhang, K. Igarashi, and K. Kikuchi, "Multi-impairment monitoring from adaptive finite-impulse-response filters in a digital coherent receiver," Opt. Express **18**, 26929–26936 (2010).
[33]X. Yi, Z. Li, Y. Bao, and K. Qiu, "Characterization of passive optical components by DSP-based optical channel estimation," IEEE Photonics Technol. Lett. **24**, 443–445 (2012).
[34]K. Kikuchi, "Electronic post-compensation for nonlinear phase fluctuations in a 1000-km 20-Gbit/s optical quadrature phase-shift keying transmission system using the digital coherent receiver," Opt. Express **16**, 889–896 (2008).
[35]A. Davis, M. Pettitt, J. King, and S. Wright, "Phase diversity techniques for coherent optical receivers," J. Lightwave Technol. **5**, 561–572 (1987).
[36]S. J. Savory, G. Gavioli, R. I. Killey, and P. Bayvel, "Electronic compensation of chromatic dispersion using a digital coherent receiver," Opt. Express **15**, 2120–2126 (2007).
[37]C. Lei, B. Guo, Z. Cheng, and K. Goda, "Optical time-stretch imaging: Principles and applications," Appl. Phys. Rev. **3**, 011102 (2016).
[38]K. Goda, D. R. Solli, K. K. Tsia, and B. Jalali, "Theory of amplified dispersive Fourier transformation," Phys. Rev. A **80**, 043821 (2009).
[39]K. Goda and B. Jalali, "Dispersive Fourier transformation for fast continuous single-shot measurements," Nat. Photonics **7**, 102–112 (2013).
[40]S. Yuan, L. Chen, Z. Wang, R. Wang, X. Wu, and X. Zhang, "Mode coupling in a terahertz multi-mode whispering-gallery-mode resonator," Opt. Lett. **44**, 2020–2023 (2019).
[41]R. L. Espinola, M. C. Tsai, J. T. Yardley, and R. M. Osgood, "Fast and low-power thermooptic switch on thin silicon-on-insulator," IEEE Photonics Technol. Lett. **15**, 1366–1368 (2003).
[42]N. Sherwood-Droz, H. Wang, L. Chen, B. G. Lee, A. Biberman, K. Bergman, and M. Lipson, "Optical 4 × 4 hitless silicon router for optical networks-on-chip (NoC)," Opt. Express **16**, 15915–15922 (2008).
[43]J. Hou, J. Dong, and X. Zhang, "Reconfigurable symmetric pulses generation using on-chip cascaded optical differentiators," Opt. Express **24**, 20529–20541 (2016).
[44]S. Yan, X. Zhu, L. H. Frandsen, S. Xiao, N. A. Mortensen, J. Dong, and Y. Ding, "Slow-light-enhanced energy efficiency for graphene microheaters on silicon photonic crystal waveguides," Nat. Commun. **8**, 14411 (2017).
[45]Y. Zhang, X. Hu, D. Chen, L. Wang, M. Li, P. Feng, X. Xiao, and S. Yu, "Design and demonstration of ultra-high-Q silicon microring resonator based on a multi-mode ridge waveguide," Opt. Lett. **43**, 1586–1589 (2018).
[46]H. Zhou, L. Chen, X. Zhou, C. Zhang, K. K. Y. Wong, and X. Zhang, "Temporal stability and spectral accuracy enhancement of the spectro-temporal analyzer," IEEE Photonics Technol. Lett. **29**, 1971–1974 (2017).